Naturally Damaged Wind Turbine Blade Bearing Fault Detection Using Novel Iterative Nonlinear Filter and Morphological Analysis

Zepeng Liu, *Student Member, IEEE*, and Long Zhang, *Member, IEEE*

***Abstract*—Wind turbine blade bearings are pivotal components to pitch blades, which optimize electrical energy output and stop wind turbines for protection. Blade bearing failure can cause the turbine to lose control or even break down. However, due to the very slow rotation speeds (often less than 5 r/min) and limited rotation angles (less than 100°), blade bearings can only produce weak and limited operating condition data, which makes condition monitoring and fault diagnosis very challenging, in particular for naturally damaged conditions. In this article, a naturally damaged large-scale blade bearing, which was in operation on a real wind farm for over 15 years, is investigated. An iterative nonlinear filter is proposed to remove heavy noise and extract weak fault vibration features. Then, the morphological transform-based envelope method is applied to diagnose the bearing fault in the frequency domain. The diagnostic results show that the proposed method can be an effective tool for diagnosing very slow speed blade bearings and is superior to some conventional bearing fault diagnosis methods.**

***Index Terms*—Blade bearing, condition monitoring and fault diagnosis (CMFD), iterative nonlinear filter (INF), morphological analysis, vibration analysis.**

I. Introduction

WIND energy is acknowledged as a sustainable and reliable energy source, which has drawn extensive attention all over the world [1]. Based on global wind statistics, the global cumulative installed wind capacity was only 23.9 GW in 2001, but it is estimated that the total capacity will reach over 800 GW by 2021 [2], [3]. Meanwhile, the single wind turbine capacity has been increased to over 10 MW. In order to optimize energy yield, modern wind turbine blades can be controlled at desired angles, while keeping the main shaft speeds within operating limits via the pitch systems. The blade bearing, also termed pitch bearing, is one of the critical components in the wind turbine pitch system, and it is a typical slewing bearing [4]. The blade bearing inner ring is connected to the blade, while the outer ring is mounted on the hub, so the bearing inner ring can be driven by electric motors (electrical pitch systems) or hydraulic equipment (hydraulic pitch systems) to change the blade pitch angle [5], [6]. However, blade bearings are usually operated in extreme and harsh environments, which can increase their failure rates [7]. The failure of blade bearings can result in lost control of blades and damage to the whole turbine system. As repair and replacement costs of failed blade bearings are high, the condition monitoring and fault diagnosis (CMFD) of blade bearings is of critical importance to decrease operation and maintenance costs, and improve system reliability [8].

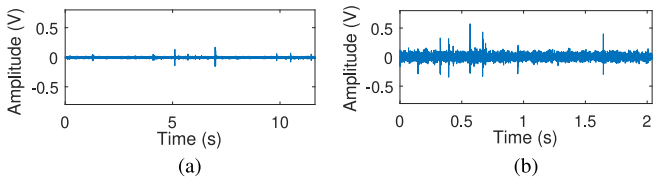

Fig. 1. Example of vibration signals with a 90° rotation angle at (a) 1.34 r/min and (b) 7.39 r/min.

To the best of the authors' knowledge, as far as the blade bearing CMFD is concerned, there is no representative publication and clear industrial standard in this field. This is because the special working mechanism of blade bearings gives rise to two main challenges, which are summarized as follows.

1) The fault signals are weak under slow rotation speed conditions (less than 5 r/min), which is due to the fact that low rotation can result in low kinetic energy according to Newton's Law. For example, Fig. 1(a) and (b) shows raw vibration signals collected from the Blade Bearing Laboratory with 90° rotation angles at 1.34 and 7.39 r/min, respectively. The weak fault signals are masked by the noise generated from bearing rotation motion, gearbox, and motor driving. Comparing Fig. 1(a) and (b), the fault signals in Fig. 1(a) at a lower rotation speed are much weaker than those in Fig. 1(b) at a higher speed.
2) The bearing rotation angle is very limited because blade bearings can only swing in small angles (less than 100°), which is different from continuously rotating main bearings, generator bearings, or gearbox bearings.

Drawing on these insights, it is very difficult to conduct blade bearing CMFD under the conditions of very low rotation speeds

Manuscript received May 13, 2019; revised August 15, 2019 and September 20, 2019; accepted October 13, 2019. Date of publication October 30, 2019; date of current version June 3, 2020. This work was supported in part by the Engineering and Physical Sciences Research Council under Grant EP/S017224/1. *(Corresponding author: Long Zhang.)*

The authors are with the Department of Electrical and Electronic Engineering, University of Manchester, M13 9PL, Manchester, U.K. (e-mail: zepeng.liu@manchester.ac.uk; long.zhang@manchester.ac.uk).

Color versions of one or more of the figures in this article are available online at http://ieeexplore.ieee.org.

Digital Object Identifier 10.1109/TIE.2019.2949522

and limited angles, because low rotation speeds result in weak fault signals masked by heavy noise, and limited angles result in a limited number of fault signals. In order to diagnose the failure type of wind turbine blade bearings, some researchers utilized fatigue life analysis to identify blade bearing health conditions [9], [10]. The aim of fatigue life analysis is to identify changes of blade bearings by comparing the conditions of deteriorated bearings with healthy bearings, so this analysis needs long-term monitoring to record both healthy and failed conditions. However, in field operations, the working conditions of new blade bearings are usually not recorded for further use. Therefore, fatigue life analysis cannot solve the two aforementioned challenges and they cannot be utilized for blade bearing CMFD. The other technique to assess health conditions of blade bearings is model-based methods [11]–[14]. Based on the inconsistency between the measured outputs of the bearings and the model-predicted outputs, the specific fault types can be inferred. However, the model-based methods often have to use physical parameters of the blade bearings which may be inapplicable in real wind turbine blade bearing fault detection. As this research is specifically concerned with blade bearing fault detection, a real wind turbine blade bearing, which had already served at a wind farm for over 15 years, is used for this article. Unlike conventional seeded defect or artificial defect bearings, this blade bearing is naturally damaged and so it demonstrates real blade bearing vibration characteristics. As a result, due to the aforementioned challenges, it is necessary to design effective methods to maximally extract and utilize the limited weak fault signals. This generally involves the techniques of signal denoising and fault characteristics analysis.

For signal denoising, the purpose is to reduce the noise components of the raw vibration signal so that the weak fault signals are extracted. As the bearing fault signals and noise components are often two uncorrelated parts [15], signal denoising can be achieved via two approaches, namely fault signal extraction and noise component elimination. With regard to the first approach, some band-pass filtering methods, such as fast kurtogram [16], can directly extract fault signals in a narrow frequency band. However, some useful frequency components beyond this frequency band are also abandoned. As a result, under slow-speed conditions, some weak fault signals may be degraded or diffused, which may affect the accuracy of the diagnostic results. The other denoising manner is noise component elimination. The noise components generated from blade bearing rotation movements have a periodic property in the time domain. The noise cancellation method, such as discrete/random separation (DRS), is to eliminate the periodic noise from raw vibration data. Then, the weak fault signals are extracted when the noise is cancelled [17], [18]. Nonetheless, in practice, the drawbacks of the noise cancellation method are that the noise components may not be completely removed and some signals (often in high frequency) may leak. Therefore, signal denoising may be unsatisfactory in some cases.

In regard to fault characteristics analysis, the envelope method is often implemented to detect the presence of defect frequencies relating to rolling elements that pass over the defect point [19]. The Hilbert transform-based envelope method (Hilbert envelope method) has been widely used in bearing fault diagnosis [20]. However, for blade bearing fault detection, the Hilbert envelope is very sensitive to noise, which can submerge weak fault signals, meaning that defect frequencies are unnoticeable in the frequency domain.

As a result, the conventional methods mentioned above may not be the ideal solutions for blade bearing fault detection because the noise level cannot be maximally suppressed. In order to minimize noise to an insignificant level and fully utilize weak fault signals, this article proposes a novel iterative nonlinear filter (INF) for signal denoising. The new INF method combines a fault signal extraction method, a nonlinear diffusion filter, and a noise cancellation method, DRS. In other words, the INF is a linear combination of a nonlinear diffusion filter and a noise cancellation filter with the aim of maximally exploiting their benefits and overcoming their weakness. This can be explained more specifically as follows.

1) The nonlinear diffusion filter was first used on image denoising and edge detection by Perona and Milik [21] and further utilized by Li *et al.* [22] as an edge-preserving denoising method for one-dimensional (1-D) signals. However, this article is the first attempt to apply nonlinear diffusion filter to bearing vibration signal denoising. The advantage of the nonlinear diffusion filter is that it can smooth the signal waveform in the time domain and directly extract weak fault signals by capturing impulse-like or sharp edge type fault signals with minimal useful information loss. This could effectively increase the defect signal-to-noise ratio.
2) The nonlinear diffusion filter may not effectively reduce periodic noise. To overcome this drawback, one possible solution is to utilize the advantage of the noise cancellation method DRS to reduce periodic noise.
3) The new INF iteratively and gradually filters the vibration signal by extracting the fault signals and cancelling out the periodic noise. The process continues until the filtering performance criterion is maximized. In this article, a kurtosis value is chosen as the criterion because a high kurtosis value can indicate that the signal has a great deal of impulsive-type fault signals.

After that, in order to diagnose the bearing fault type in the frequency domain, the morphological transform-based envelope method (morphological envelope method) is employed for fault characteristic analysis. The morphological transform is a nonlinear analysis method, which was first utilized to denoise images [23]. Then, Nikolaou *et al.* [24] developed the morphological transform for bearing vibration signal envelope analysis. Unlike the conventional Hilbert envelope method, the morphological envelope method can further denoise the residual noise leaked from the INF filter and enhance the weak fault signals, so the bearing defect frequencies can be identified distinctly. Extensive experimental results demonstrate that the proposed INF and morphological envelope methods outperform conventional filtering methods or the Hilbert envelope method

when diagnosing the naturally damaged slow speed blade bearing fault type.

The main contributions of this article can therefore be summarized as follows.

1) First, a new filter method INF is proposed to overcome the drawbacks of the nonlinear diffusion filter and DRS method, and it outperforms conventional filtering methods.
2) Second, to the best of the authors' knowledge, it is the first time the diagnosis of naturally damaged wind turbine blade bearings has been carried out.
3) Finally, blade bearings operate under unique working conditions, including both slow rotation speeds and limited rotation angles. These result in weak and limited vibration data. Nonetheless, our proposed method can effectively overcome these two challenges, which is demonstrated in a laboratory setting.

The rest of this article is organized as follows. In Section II, the theoretical background of bearing defect frequencies, INF and morphological analysis are discussed in details. Then, Section III is dedicated to a description of the performed experiments and diagnostic results. Finally, Section IV concludes this article.

II. Theoretical Background

A. Bearing Defect Frequencies

A wind turbine blade bearing is made up of the outer race, inner race, and balls. Balls rolling over the local defects in the bearing can generate a sequence of impacts. The repetition rate of these impacts is defined as the bearing defect frequency, which can be calculated by the mechanical dimensions of the bearing [6], [25]

$$f_o = (N_b/2) \cdot (1 - d_b \cdot \cos\alpha/d_p) \cdot f_r \tag{1}$$

$$f_i = (N_b/2) \cdot (1 + d_b \cdot \cos\alpha/d_p) \cdot f_r \tag{2}$$

$$f_b = (d_p/2d_b) \cdot \left(1 - (d_b \cdot \cos\alpha/d_p)^2\right) \cdot f_r \tag{3}$$

where f_o indicates the outer race defect frequency, f_i is defined as the inner race defect frequency, and f_b is defined as the balls defect frequency. f_r is the rotational frequency of the bearing. N_b is the number of rolling elements; d_b is the rolling element diameter; d_p is the pitch diameter; and α is the contact angle.

In the frequency domain, if one of the bearing defect frequencies matches one or more dominant frequencies of the vibration signal, a specific fault in the bearing can be inferred.

B. Iterative Nonlinear Filter

The new denoising method INF is a linear combination of a nonlinear diffusion process and a noise cancellation process, which can iteratively and gradually smooth the signal waveform and remove periodic noise. On the one hand, if only the nonlinear diffusion process is applied, the signal waveform, which is influenced by the high frequency signal, can be smoothed but the periodic noise cannot be removed; on the other hand, if only the noise cancellation method DRS is adopted, the periodic noise can be eliminated but the high frequency signals may leak. As a result, the combination of the nonlinear diffusion process and DRS can fully exploit their benefits and overcome their weaknesses.

1) Nonlinear Diffusion Process: The main idea of INF is the nonlinear diffusion filter, which is a multiscale smoothing and impulse signal detection scheme [26]. In other words, the nonlinear diffusion filter can reduce noise and extract impulsive-type fault signals with minimal useful information loss. The nonlinear diffusion filter is summarized as follows.

Let $X(n)$ be a raw vibration signal of length N. The equation for the nonlinear diffusion process based on the Perona-Malik model is expressed as follows [21]:

$$\frac{\partial}{\partial \mathrm{t}} X(n,t) = \frac{\partial}{\partial n}\left[c(n,t) \cdot \frac{\partial}{\partial n} X(n,t)\right] \tag{4}$$

with an initial condition $X(n,0) = X(n), n = 1, \ldots, N$. $c(n,t)$ indicates the diffusion function, which controls the diffusion strength and denoising strength, and $X(n,t)$ is the current signal intensity. The variable t is the process ordering parameter.

The diffusion function $c(n,t)$ varies with the magnitude of the gradient of the signal intensity $X(n,t)$, which is a monotonically decreasing function $c(n,t) = f(\frac{\partial}{\partial n} X(n,t))$. In general, $c(0,t) = 1$ and $c(n,t) > 0$ for n tending to infinity. The diffusion function is expressed in the following:

$$c(n,t) = \exp\left(-\left(\left|\frac{\partial}{\partial n} X(n,t)\right| \Big/ \kappa\right)^2\right) \tag{5}$$

where the parameter κ is the noise threshold. If $\frac{\partial}{\partial n} X(n,t)$ is large, $c(n,t)$ becomes small, which indicates the diffusion is weak and the spikes can be prevented. On the contrary, if $\frac{\partial}{\partial n} X(n,t)$ is small, $c(n,t)$ is large; therefore, the diffusion is strong, which can smooth the signal waveform.

In order to find the solution for the nonlinear diffusion equation, the discrete approximation is considered. For one iteration step of (4), the expression of $\frac{\partial}{\partial t} X(n,t)$ and $\frac{\partial}{\partial n} X(n,t)$ are, respectively, approximated as [22]

$$\frac{\partial}{\partial t} X(n,t) \approx \frac{X(n, t+\Delta t) - X(n,t)}{\Delta t} \tag{6}$$

and

$$\frac{\partial}{\partial n} X(n,t) \approx \frac{X(n+\Delta n/2, t) - X(n-\Delta n/2, t)}{\Delta n}. \tag{7}$$

Moreover, the discrete approximation of $\frac{\partial}{\partial n}[c(n,t) \cdot \frac{\partial}{\partial n} X(n,t)]$ is [26]

$$\begin{aligned}
&\frac{\partial}{\partial n}\left[c(n,t) \cdot \frac{\partial}{\partial n} X(n,t)\right] \\
&\approx \frac{\partial}{\partial n}\left[c(n,t) \cdot \frac{1}{\Delta n}\left(X\left(n + \frac{\Delta n}{2}, t\right) - X\left(n - \frac{\Delta n}{2}, t\right)\right)\right] \\
&\approx \frac{1}{\Delta n^2}\left[c\left(n + \frac{\Delta n}{2}, t\right) \cdot (X(n+\Delta n, t) - X(n,t))\right. \\
&\qquad \left. - c\left(n - \frac{\Delta n}{2}, t\right) \cdot (X(n,t) - X(n-\Delta n, t))\right] \\
&= \Phi_r - \Phi_l
\end{aligned} \tag{8}$$

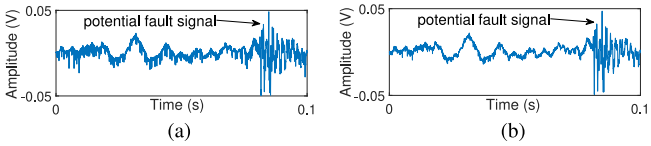

Fig. 2. (a) Enlarged raw vibration signal within 0.1 s. (b) Nonlinear diffusion filtered signal after the first iteration.

where $\Phi_r = \frac{1}{\Delta n^2} \cdot c(n + \frac{\Delta n}{2}, t) \cdot (X(n + \Delta n, t) - X(n, t))$ and $\Phi_l = \frac{1}{\Delta n^2} \cdot c(n - \frac{\Delta n}{2}, t) \cdot (X(n, t) - X(n - \Delta n, t))$.

Substituting (6) and (8) into (4), yields

$$X(n, t + \Delta t) - X(n, t) = (\Phi_r - \Phi_l) \cdot \Delta t. \tag{9}$$

For convenience, denoting $\mathrm{X}^{k+1}(n)$ and $\mathrm{X}^{k}(n)$ to $X(n, t + \Delta t)$ and $X(n, t)$, respectively, therefore, the next iteration can be expressed as:

$$\mathrm{X}^{k+1}(n) = \mathrm{X}^{k}(n) + \Delta t \cdot (\Phi_r - \Phi_t) \tag{10}$$

where $X^k(n)$ indicates the nonlinear diffusion filtered signal at the kth iteration.

For example, Fig. 2(a) shows an enlarged raw vibration signal within 0.1 s. After the first iteration shown in Fig. 2(b), the edge of the signal waveform has been smoothed and the potential fault signal is preserved; therefore, the contrast between weak fault signals and the signal waveform is increased so that the defect signal-to-noise ratio is increased.

2) Noise Cancellation Process: After the signal waveform is smoothed via the nonlinear diffusion filter, the next step of INF is to eliminate periodic noise via the noise cancellation process. As mentioned in the introduction part, fault signals and noise components are often two uncorrelated parts, so the expression of the nonlinear diffusion filtered signal $X^k(n)$ at the kth iteration can be expressed as $X^k(n) = p^k(n) + r^k(n), n = 1, \ldots, N$ where $p^k(n)$ represents a periodic process, including noise components and $r^k(n)$ represents a stochastic process containing bearing faults [17]. $r^k(n)$ and $p^k(n)$ are independent with each other. Based on the prediction theory, the periodic process can be predicted using past values, while the stochastic part cannot be predicted from its previous values, which is estimated from the prediction error [17].

More specifically, from [17], define $\widehat{X}^k(n)$ as the predictor of $X^k(n)$ from a finite number of past values $X^k(n - \Lambda - i)$, where $i = 0, \ldots, M - 1$ with Λ satisfies the autocorrelation equation $\mathbb{E}[r^k(n)r^k(n - \lambda)] = 0$ for all $|\lambda| > \Lambda$. The notation $\mathbb{E}[.]$ is the expectation operator. The expression of $\widehat{X}^k(n)$ is given by a linear regressor of the form

$$\widehat{X}^k(n) = \sum_{i=0}^{M-1} h_i^k X^k(n - \Lambda - i). \tag{11}$$

Therefore, from the abovementioned discussion, the estimator of the periodic process is $\widehat{p}^k(n) = \widehat{X}^k(n)$; and the prediction error, which is the estimator of the stochastic process is expressed as $\widehat{r}^k(n) = \widehat{X}^k(n) - X^k(n)$. In order to find the best $\widehat{X}^k(n)$ that can minimize the prediction error $\widehat{r}^k(n)$, the following mean squared error σ_e^2 is used:

$$\sigma_e^2 = \frac{1}{N} \sum_{n=1}^{N} \left[\widehat{X}^k(n) - X^k(n)\right]^2. \tag{12}$$

To find out the minimum σ_e^2, we can compute the gradient of (12)

$$\sum_{i=1}^{M-1} \frac{\partial\left(\sigma_e^2\right)}{\partial h_i^k} = \frac{2}{N} \sum_{n=1}^{N} \left[\sum_{i=0}^{M-1} h_i^k r^k(n, i) - r^k(n)\right] \tag{13}$$

where $r^k(n, i) = \sum_{j=0}^{M-1} X^k(n - \Lambda - j)X^k(n - \Lambda - i)$ and $r^k(n) = \sum_{j=0}^{M-1} X^k(n - \Lambda - j)X^k(n)$. Then, at the minimum, the condition that should hold is $\sum_{i=0}^{M-1} h_i^k r^k(n, i) - r^k(n) = 0$. Finally, the optimal set of weights h_i^k, $i = 0, \ldots, M - 1$ verifies the Wiener–Hopf equations

$$r^k(n) = \sum_{i=0}^{M-1} h_i^k r^k(n, i), n = 1, \ldots, N. \tag{14}$$

Antoni *et al.* [18] proposed a faster approach DRS to process (14) in the frequency domain

$$\mathscr{F}\left[r^k(n)\right] = R_1^k(f) = \mathscr{F}\left[\sum_{i=0}^{M-1} h_i^k r^k(n, i)\right]$$
$$= \sum_{n=1}^{N} r^k(n, i) e^{-j\omega(n-i)} \sum_{i=0}^{M-1} h_i^k e^{-j\omega i} = R_2^k(f) H^k(f) \tag{15}$$

where $\mathscr{F}[.]$ corresponds to the discrete Fourier transform (DFT). As can be seen in (15), the Wiener–Hopf equation is simplified into the product and the filter $H^k(f)$ can be solved via a current signal block $R_1^k(f)$ and a past signal block $R_2^k(f)$. Assuming $R_1^k(f) = \mathscr{F}[X^k(n - \xi)]$ and $R_2^k(f) = \mathscr{F}[X^k(n - \Delta - \xi)]$ where $\xi = 0, \ldots, \Xi - 1$ and $\Delta > 0$. Labeling $\widehat{r}_\Phi^k(f)$ and $\widehat{R}_\Phi^{k,\Delta}(f)$ are the estimators of $R_1^k(f)$ and $R_2^k(f)$, respectively, which are the Φ-long ($\Phi = 2\Xi$ due to possible zero padding) DFT of the two blocks at frequency f, the estimator of $H^k(f)$ is given by [18]

$$\widehat{H}^k(f) = \widehat{R}_\Phi^{k,\Delta}(f) \cdot \widehat{R}_\Phi^k(f)^* \Big/ \left|\widehat{R}_\Phi^{k,\Delta}(f)\right|^2. \tag{16}$$

The estimator $\widehat{H}^k(f)$ is a Φ-long noise cancellation filter, which can be used directly on the kth iteration signal denoising. Finally, the INF filtered signal $X_D^k(n)$ at kth iteration can be expressed as

$$X_D^k(n) = X^k(n) * \widehat{h}^k(\phi), \phi = 1, \ldots, \Phi \tag{17}$$

where $\widehat{h}^k(\phi) = \mathscr{F}^{-1}(\widehat{H}^k(f))$ and $\mathscr{F}^{-1}[.]$ corresponds to the inverse DFT, and $*$ indicates the convolution.

If the noise reduction of $X_D^k(n)$ is unsatisfactory, it can be substituted into (10) for the next iteration of denoising. Fig. 3 shows a real example to illustrate the INF denoising procedure. In Fig. 3(b), there is remarkable noise after the first INF iteration and the kurtosis is only 69.28. After nine iterations shown in Fig. 3(c), the noise level has been reduced gradually with the kurtosis varying from 69.28 to 1076.61.

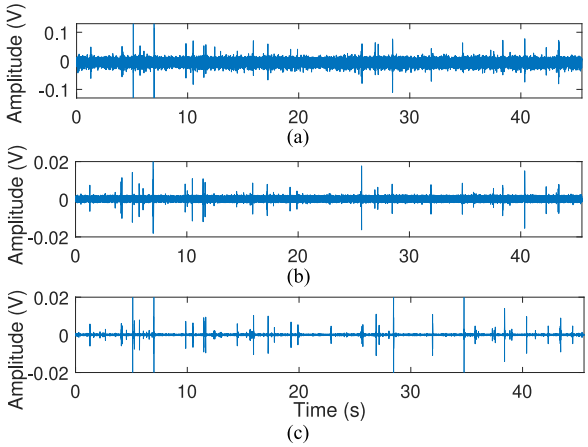

Fig. 3. (a) Raw vibration signal, and INF denoised signals after the (b) first INF iteration and (c) ninth INF iteration.

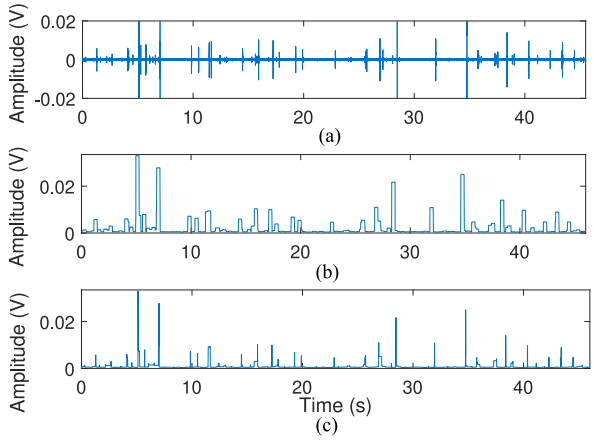

Fig. 4. (a) INF denoised signal, and different kinds of morphological envelopes. (b) Dilation. (c) Closing.

C. Morphological Analysis

The vibration signals are characterized by the presence of impulsive-type fault signals modulated by high-frequency harmonic components [24]. However, for bearing fault characteristic analysis, the useful information is only the repetition rate of these impulsive-type fault signals (this is also referred to as the defect frequency), rather than detailed frequency contents of the full signal. To extract this repetition rate, morphological analysis is employed in this article as it can extract impulsive-type fault signals and eliminate the impact of background noise. The implementation of morphological analysis is based on two basic set operations: Minkowski set addition [also termed dilation shown in (18)] and Minkowski set subtraction [also termed erosion shown in (19)] [24].

$$\left(X_D^k \oplus S\right)(n) = \max\left[X_D^k(n-\tau) + S(\tau)\right] \tag{18}$$

$$\left(X_D^k \ominus S\right)(n) = \min\left[X_D^k(n+\tau) - S(\tau)\right] \tag{19}$$

where $\ominus$ indicates the operation of erosion and $\oplus$ represents the operation of dilation. $X_D^k(n)$ is the INF denoised signal after kth iteration with $n = 1, \ldots, N$; and the discrete function $S(\tau)$ is the structuring element (SE) over a domain $\tau = 1, \ldots, \mathrm{T}$ with $\mathrm{T} < \mathrm{N}$.

The combinations of the aforementioned two operations can demodulate two other signal envelopes: Closing and opening. For example, to get the morphological closing envelope, the vibration signal is first added with the SE through the operation of Minkowski set addition and then subtracted with the SE through Minkowski set subtraction [24]. As for the operation of opening, the order of the set addition and set subtraction is reversed. The equations are as follows:

$$\left(X_D^k \bullet S\right)(n) = \left(X_D^k \oplus S \ominus S\right)(n) \tag{20}$$

$$\left(X_D^k \circ S\right)(n) = \left(X_D^k \ominus S \oplus S\right)(n) \tag{21}$$

where $\circ$ and $\bullet$ indicates the operation of opening and closing.

Equations (18)–(21) can plot four types of envelopes, and here we will demonstrate dilation and closing as examples. The INF denoised signal [shown in Fig. 4(a)] can be further processed via dilation and closing presented in Fig. 4(b) and (c). As can be seen, the morphological transform can further reduce the residual noise leaked from the INF processing. Comparing dilation and closing, it is observed that the closing of the signal presents a better visual inspection, whose shape is more close to the bearing fault signals. With respect to erosion and opening, they can only demonstrate negative impulses; for our research, we prefer to use the positive envelope. Therefore, in this article, we employ the closing of the signal as the morphological closing envelope, which is used for fault characteristics analysis. Finally, the frequency spectrum of the morphological closing envelope $\mathscr{F}[(X_D^k \bullet S)(n)]$ is calculated to identify the bearing defect frequencies.

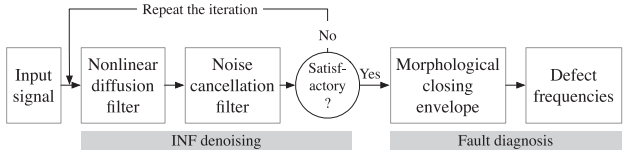

Fig. 5. Flowchart of the proposed method.

D. Summary of the Algorithm and Parameter Tuning

As can be seen in the flowchart (see Fig. 5), the procedure of the blade bearing fault detection is conducted in two stages: The INF denoising stage and the fault diagnosis stage. The INF denoising stage produces an iterated processing scheme to gradually denoise the raw vibration signal until noise reduction reaches a satisfactory level. The morphological analysis is then used to detect bearing defect frequencies.

For the INF denoising stage shown in Fig. 5, each iteration consists of two steps: smoothing via a nonlinear diffusion process and periodic noise elimination via a noise cancellation process. With respect to the nonlinear diffusion process, the integration constant Δt is the first parameter that has to be determined. For the 1-D case, Gerig *et al.* [26] derived the upper bound of Δt up to $\frac{1}{3}$; therefore, in this article, $\Delta t = \frac{1}{3}$ is used. The other important parameter is the noise threshold κ, which controls the amount of diffusion applied in the gradient

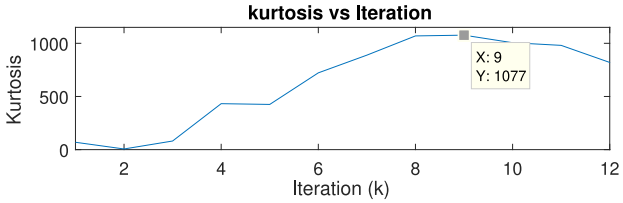

Fig. 6. Kurtosis versus iteration k.

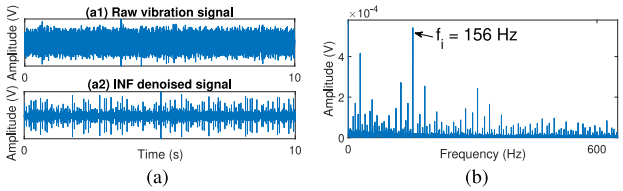

Fig. 7. High-speed bearing (a1) raw vibration signal, (a2) INF denoised signal, and (b) frequency spectrum processed by morphological envelope method.

direction [27]. The selection of κ is based on trial and error. To obtain a better denoising performance, a test series with different κ must be generated and compared. Concerning the DRS noise cancellation process, the filter length Φ can influence the quality of the denoised signal and it should exceed a potential fault signal length. The second parameter of DRS is to choose a suitable time delay Δ. The optimal value of Δ can enable the constructed filter to minimize the mean squared error shown in (12). The value of Δ can be incrementally increased and the one with the least mean squared error is chosen. The last parameter for INF denoising is the number of iterations k. To evaluate the denoising performance for each iteration, the kurtosis is preferred as an indicator. The iteration continues until the maximal kurtosis value is found. For example, as can be seen in Fig. 6, the highest kurtosis is 1077 at Iteration 9. Therefore, we can repeat nine times to denoise the raw vibration signal.

With respect to the fault diagnosis stage in Fig. 5, flat SEs (e.g., amplitude = 0) are utilized in this article. Therefore, the length of the SE is the only tunable factor for morphological analysis. Generally speaking, a shorter SE can extract more signal impulses enhancing higher frequency components. On the contrary, a longer SE can extract a smaller number of spikes enhancing lower frequency components. A proper SE can help produce defect frequency accurately in terms of both frequency components and amplitude. When changing the length of SE, each extracted defect frequency can be compared with the theoretical defect frequency. The SE value that produces the distinct defect frequency will be used.

E. Validation on a Small-Scale Bearing

In this subsection, we aim to evaluate the effectiveness of the INF and morphological analysis on a widely used small-scale bearing with a seeded inner race fault from the SpectraQuest Machinery Fault Simulator test rig [28]. The theoretical inner race defect frequency is 157.4 Hz. After applying INF to the raw vibration signal [see Fig. 7(a1)], the denoised signal shown in Fig. 7(a2) can clearly present the submerged bearing fault

TABLE I
BEARING DEFECT FREQUENCIES

Test	Rotation speeds (rpm)	f_i (Hz)	f_o (Hz)	f_b (Hz)
Test 1	2.13	1.1019	1.0279	0.3282
Test 2	1.27	0.6569	0.6129	0.1957

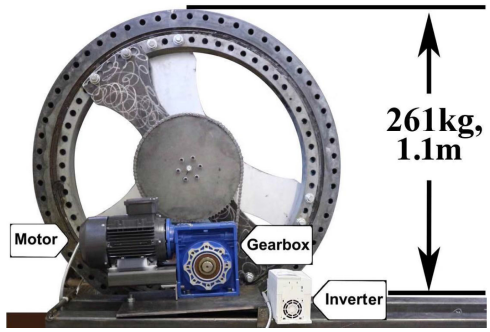

Fig. 8. Wind turbine blade bearing test rig.

signals. Furthermore, morphological envelope analysis is utilized in order to present the bearing defect frequency. It can be found in Fig. 7(b), the dominant frequency component is 156 Hz, which corresponds to the bearing inner race fault frequency. As a result, this validation experiment demonstrates that our proposed method is effective and accurate.

III. EXPERIMENT AND RESULTS

The test wind turbine blade bearing was manufactured by Rollix, and was operational on a wind farm for over 15 years. The defects of the bearing were therefore naturally damaged under real wind turbine working conditions. The weight of this bearing is 261 kg and its pitch diameter, ball diameter, ball numbers, and contact angle are 1000 mm, 54 mm, 60 and 50°, respectively. Based on these geometric parameters, the bearing defect frequencies are calculated using (1)–(3), and are listed in Table I.

In order to diagnose the failure type of this blade bearing, the bearing test rig is designed, as shown in Fig. 8. The outer ring of the bearing is vertically connected to the test rig; therefore, the bearing inner ring can be rotated. The kinematic components of the test rig contain the three-phase induction motor, gearbox, chain, and blade bearing. During the experiment, the motor can drive the bearing to rotate via the chain drive system; and the bearing rotation speed is controllable via a motor inverter. Finally, a tachometer is used to measure the rotating speed of the gearbox. According to the teeth ratio of the driven sprocket connected to the bearing and the driving sprocket connected to the gearbox, the bearing rotation speed can be calculated.

For real-world blade bearing operations, shown in Fig. 9, the bearing can slowly swing back and forth within 100°; and rotation speeds can be controlled from 1 to 2.5 r/min. The launching and ending periods are inconstant, and only the middle period, e.g., 90°, is constant or quasi-constant. In order to simulate real-world blade bearing working conditions, the test bearing is designed to swing back and forth within 100° as shown

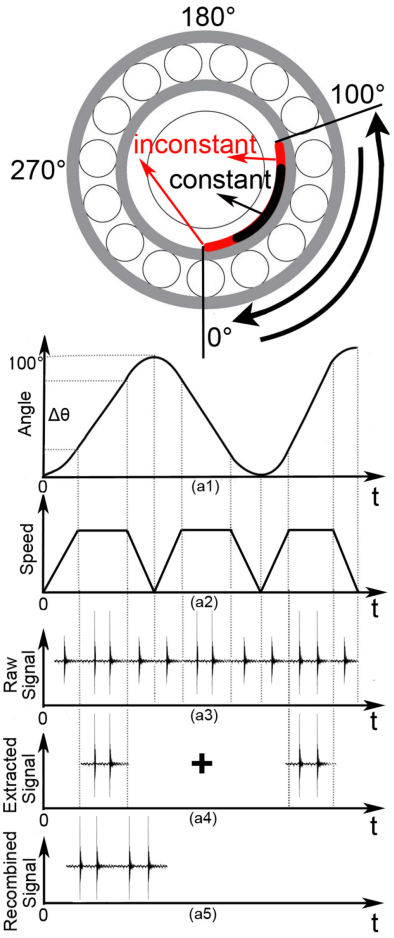

Fig. 9. Schematics of wind turbine blade bearing field operation.

in Fig. 9; and we only use a part of the data per revolution [see Fig. 9(a4)]. These same constant speed short parts can be recombined to increase the data length in order to improve the diagnostic accuracy [see Fig. 9(a3)–(a5)].

Vibration signals of the blade bearing shown in Fig. 8 are collected from accelerometers installed on the bearing outer ring surface. The accelerometers are Hansford HS-100-type sensors with 1000 mV/g sensitivity and constant frequency gain between 2 to 10 kHz. Based on the schematic shown in Fig. 9, Fig. 10(a) shows Test 1 raw vibration data at a sampling rate of 100 kS/s. The bearing rotating process includes accelerating, constant speed, and decelerating within 100°. Fig. 10(b) shows the recombined signals with four 90° portions of vibration data. Each part is extracted from each revolution and the extracted parts have similar vibration characteristics with the rotation speed of 2.13 r/min. As can be seen, the kurtosis of the recombined raw signal is only 125.46. The new INF is a combination of the nonlinear diffusion filter and DRS method. To demonstrate its performance, only the nonlinear diffusion filter is first utilized to denoise the recombined signal. After carefully tuning the parameters, the kurtosis of the nonlinear diffusion denoised signal decreases to 124.28 [see Fig. 10(c)].

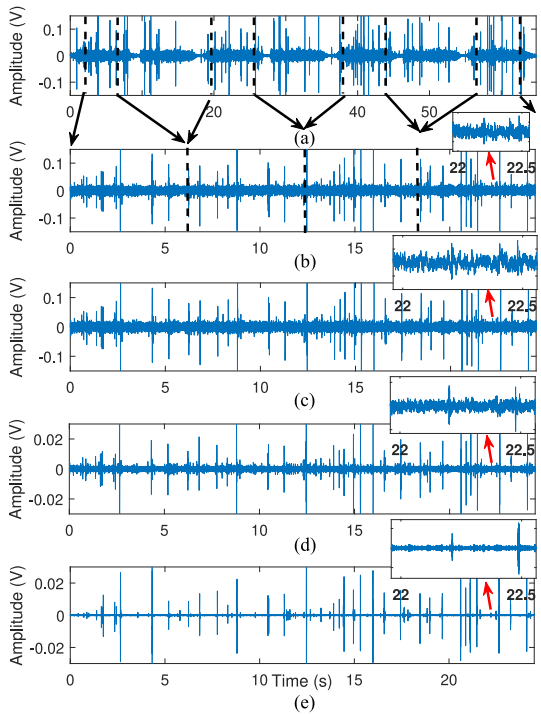

Fig. 10. Test 1. (a) Raw vibration signal collected under the reciprocating operation condition. (b) Recombined signal at 2.13 r/min. (c) Nonlinear diffusion denoised signal. (d) DRS denoised signal. (e) INF denoised signal.

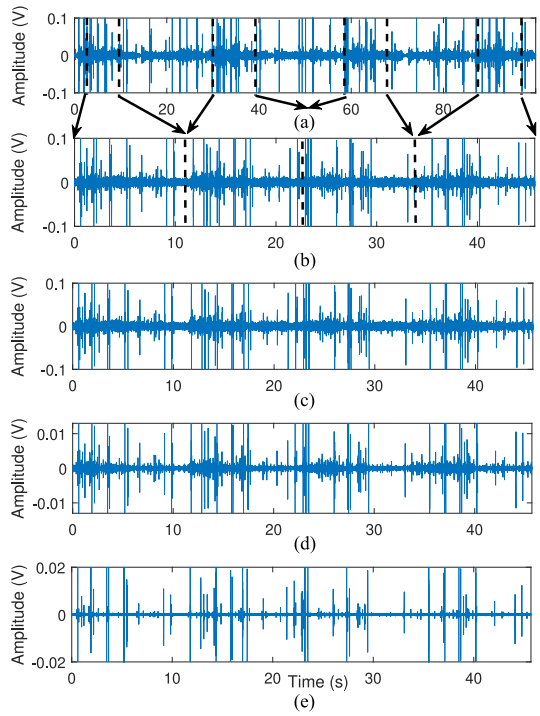

Fig. 11. Test 2. (a) Raw vibration signal collected under the reciprocating operation condition. (b) Recombined signal at 1.27 r/min. (c)Nonlinear diffusion denoised signal. (d) DRS denoised signal. (e) INF denoised signal.

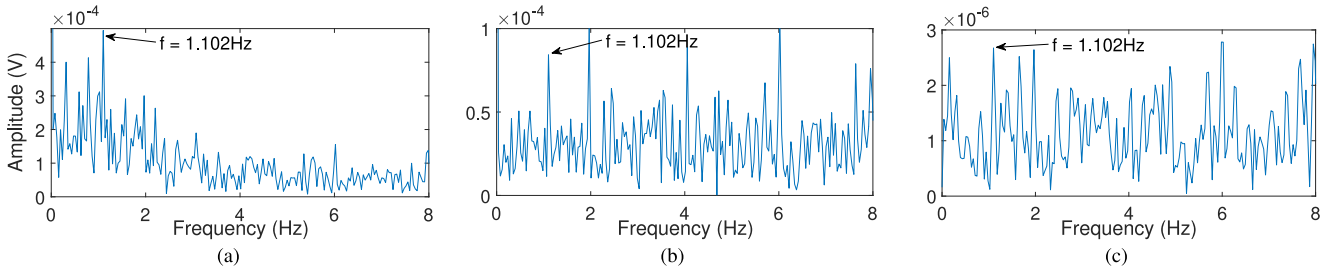

Fig. 12. Test 1 at 2.13 r/min, frequency spectrums processed by (a) INF/morphological closing envelope method, (b) INF/Hilbert envelope method, and (c) fast kurtogram/Hilbert envelope method.

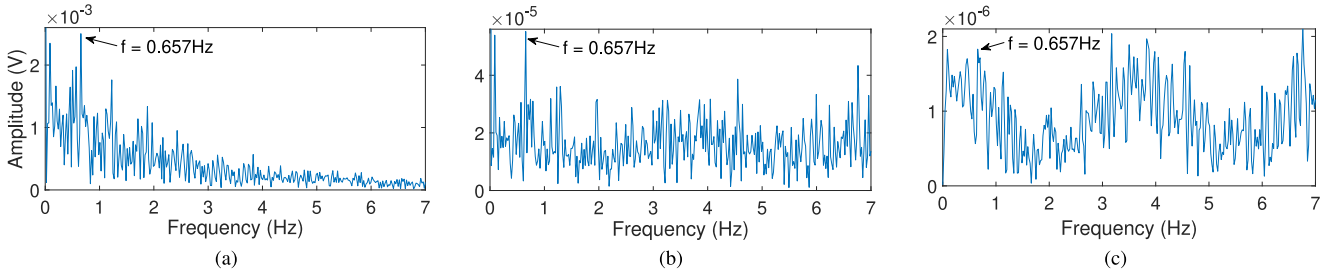

Fig. 13. Test 2 at 1.27 r/min, frequency spectrums processed by (a) INF/morphological closing envelope method, (b) INF/Hilbert envelope method, and (c) fast kurtogram/Hilbert envelope method.

Then, we utilize DRS to denoise the recombined signal. As can be seen in Fig. 10(d), the kurtosis of the DRS denoised signal improves to 397.95. However, some weak fault signals are still corrupted by noise. In order to overcome this issue, the proposed INF method is then used, with the denoised signal shown in Fig. 10(e). Compared with the DRS denoised signal, Fig. 10(e) shows very low noise interference, with the kurtosis of the filtered signal improving to 1492.08. In order to show the effectiveness of the INF method, some enlarged signals from 22 to 22.5 s are shown in Fig. 10(b)–(e). It can be clearly seen that the new INF method can produce better filtering results with clearer defect signals than the nonlinear diffusion filter and DRS method.

With regard to Test 2, Fig. 11(a) shows the raw vibration signal, where the constant part has a speed of 1.27 r/min. Fig. 11(b) shows the recombined signal. As can be seen in Fig. 11(b), the kurtosis of the recombined raw signal is 317.34. Then, we utilize nonlinear diffusion filter to denoise the recombined signal and the kurtosis value decreases to around 315.44 [see Fig. 11(c)]. After applying DRS to filter the recombined signal, the kurtosis value improves to 687.09 [see Fig. 11(d)]. In order to further denoise the recombined signal and extract weak fault signals, the novel INF is utilized. As shown in Fig. 11(e), the compounded fault signals are clearly presented with minimal noise interference and the kurtosis value improves from 317.34 to 1124.23.

The second stage is to extract morphological closing envelopes with the aim of finding defect frequencies in the frequency domain. The morphological closing envelope modifies the geometrical characteristics by morphologically processing the signal which can further extract impulsive-type fault signals. After applying FFT to the morphological closing envelopes, the dominant frequencies are 1.102 Hz for 2.13 r/min and 0.657 Hz for 1.27 r/min shown in Figs. 12(a) and 13(a), respectively.

As our proposed blade bearing diagnostic method has two parts containing INF filtering and morphological envelope analysis, in order to evaluate the performance of the proposed method, some comparisons with Hilbert envelope method and conventional band-pass filtering method are carried out. Figs. 12(b) and 13(b) show the combination of INF and the Hilbert envelope method. Although this method can show defect frequencies, some other unknown frequency components are also presented, meaning that the defect frequencies are disturbed.

Figs. 12(c) and 13(c) demonstrate the frequency spectrum processed by the fast kurtogram analysis [16]. As can be seen, the defect frequencies are relatively weaker and harder to distinguish when compared with the results produced by the new method.

The following equation is used to evaluate the defect frequency matching error (DFME), which is the ratio between the identified dominant frequency and the theoretical defect frequency:

$$\text{Error} = \left(\left|f_{\text{rotation}} - f_{\text{fault}}\right| / f_{\text{fault}}\right) \times 100\% \tag{22}$$

where f_{rotation} indicates the dominant frequencies for each test and f_{fault} can be chosen as f_i, f_o, and f_b shown in Table I. Table II lists the DFME of Test 1 and Test 2. It is found that the bearing most likely has an inner race fault with an average matching error of 0.05%. To further evaluate our proposed method, the authors conduct extensive experiments to simulate different slow-speed and limited angle cases. As shown in Table III, the bearing defect frequencies can be identified and they all match the theoretical

TABLE II
DFME OF TEST 1 AND TEST 2

Test	rpm	Inner race fault	Outer race fault	Ball race fault
Test 1	2.13	0.10%	7.21%	235.77%
Test 2	1.27	0.01%	7.20%	235.71%
	Average	**0.05%**	7.20%	235.74%

TABLE III
DFME OF EXTENSIVE EXPERIMENTS

Rotation speeds (rpm)	1.07	1.31	2.14	2.21	3.10	3.12
Identified defect frequency (Hz)	0.552	0.666	1.106	1.116	1.602	1.612
Inner race DFME	**0.13%**	**1.65%**	**0.09%**	**2.38%**	**0.10%**	**0.12%**
Outer race DFME	7.05%	5.42%	7.09%	4.64%	7.08%	7.06%
Balls DFME	235.2%	230.1%	235.3%	227.6%	235.3%	235.2%

The bold font indicates that the identified defect frequencies match the theoretical inner race defect frequencies with smallest matching errors.

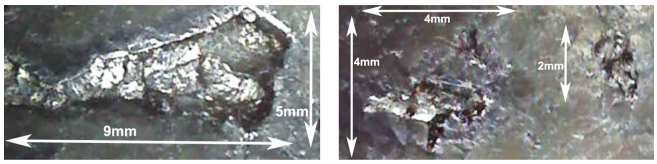

(a) (b)

Fig. 14. Visible inner race defects. (a) First position. (b) Second position.

inner race defect frequencies with smallest defect frequency matching errors.

Finally, endoscope inspection is used to collect the evidence of bearing damages. Two pictures have been taken in order to indicate the presence of some cracks in the inner race. Fig. 14(a) shows the first position, which has a large crack, with dimensions of over 9 mm long and 5 mm wide. From Fig. 14(b), the second position presents some smaller cracks, which are less than 4 mm. Therefore, the inner race damage evidences verify that the proposed methods are capable of detecting blade bearing damages. However, it is worth mentioning that when a bearing inner race is severely damaged, the balls and outer race may not be in perfect condition. In this article, the endoscope also checks the outer race and balls, where no obvious damage is found except for some tiny dents. Compared with the visible damage to the inner race, the damage to the balls and the outer race is insignificant.

IV. CONCLUSION

This article diagnosed a naturally damaged wind turbine blade bearing. The blade bearing pitch processes include launching periods, constant speeds and ending periods. To avoid the non-stationary signals caused by launching and ending periods, the work of this article was to diagnose the blade bearing fault types when the signals generated from launching and ending periods are abandoned, and only constant rotation parts are utilized. As blade bearings rotate at very slow speeds within small angles, vibration signals are short and weak. To improve the diagnostic accuracy, we first recombined the segmented constant speed short parts to extend the data length. Then, a novel INF was proposed to iteratively and gradually smooth the signal waveform and extract weak fault signals. Finally, the morphological closing envelope method was used to diagnose the bearing fault in the frequency domain. The proposed method was successfully applied to diagnose a naturally damaged blade bearing under different slow-speed conditions and it was effective and superior to other conventional filtering methods or the Hilbert envelope method. In future research activities, we will research the blade bearing fault detection under variable speed conditions and loading conditions.

ACKNOWLEDGMENTS

The authors would like to thank Acciona for providing the bearings for the work. The authors would like to thank the Editor and anonymous reviewers for their constructive comments to improve the quality of this article.

REFERENCES

[1] B. Yang, R. Liu, and X. Chen, "Fault diagnosis for a wind turbine generator bearing via sparse representation and shift-invariant K-SVD," *IEEE Trans. Ind. Inform.*, vol. 13, no. 3, pp. 1321–1331, Jun. 2017.
[2] Y. Xiao, N. Kang, Y. Hong, and G. Zhang, "Misalignment fault diagnosis of DFWT based on IEMD energy entropy and PSO-SVM," *Entropy*, vol. 19, no. 1, pp. 6–12, 2017.
[3] Z. Liu and L. Zhang, "A review of failure modes, condition monitoring and fault diagnosis methods for large-scale wind turbine bearings," *Measurement*, vol. 149, p. 107002, 2019.
[4] L. Chen, Y. Zhang, and X. Xia, "Contact stress and deformation of blade bearing in wind turbine," in *Proc. Int. Conf. Measuring Technol. Mechatronics Autom.*, vol. 1, Mar. 2010, pp. 833–836.
[5] M. H. Larsen, A. V. Nielsen, and S. F. Poulsen, "Pitch bearing for wind turbine rotor blades," U.S. Patent 8,322,928, Dec. 4, 2012.
[6] Z. Liu, L. Zhang, and J. Carrasco, "Vibration analysis for large-scale wind turbine blade bearing fault detection with an empirical wavelet thresholding method," *Renewable Energy*, vol. 146, pp. 99–110, 2020.
[7] J. Wang, Y. Peng, and W. Qiao, "Current-aided order tracking of vibration signals for bearing fault diagnosis of direct-drive wind turbines," *IEEE Trans. Ind. Electron.*, vol. 63, no. 10, pp. 6336–6346, Oct. 2016.
[8] L. Zhang, Z. Q. Lang, and M. Papaelias, "Generalized transmissibility damage indicator with application to wind turbine component condition monitoring," *IEEE Trans. Ind. Electron.*, vol. 63, no. 10, pp. 6347–6359, Oct. 2016.
[9] J. W. Han, J. S. Nam, Y. J. Park, G. H. Lee, and Y. Y. Nam, "An experimental study on the performance and fatigue life of pitch bearing for wind turbine," *J. Mech. Sci. Technol.*, vol. 29, no. 5, pp. 1963–1971, 2015.
[10] Y. Wang and Q. Yuan, "Static load-carrying capacity and fatigue life of a double row pitch bearing with radial interference," *Proc. Institution Mech. Engineers, Part C: J. Mech. Eng. Sci.*, vol. 228, no. 2, 2014, pp. 307–316.
[11] Y. Wang, X. Yang, and H. Yan, "Reliable fuzzy tracking control of near-space hypersonic vehicle using aperiodic measurement information," *IEEE Trans. Ind. Electron.*, vol. 66, no. 12, pp. 9439–9447, Dec. 2019.
[12] Y. Wang, P. Shi, and H. Yan, "Reliable control of fuzzy singularly perturbed systems and its application to electronic circuits," *IEEE Trans. Circuits Syst. I: Regular Papers*, vol. 65, no. 10, pp. 3519–3528, Oct. 2018.
[13] Y. Xiao, T. Zhang, Z. Ding, and C. Li, "The study of fuzzy proportional integral controllers based on improved particle swarm optimization for permanent magnet direct drive wind turbine converters," *Energies*, vol. 9, no. 5, p. 343, 2016.
[14] B. Yang, R. Liu, and E. Zio, "Remaining useful life prediction based on a double-convolutional neural network architecture," *IEEE Trans. Ind. Electron.*, vol. 66, no. 12, pp. 9521–9530, Dec. 2019.
[15] W. Zhou, T. G. Habetler, and R. G. Harley, "Bearing fault detection via stator current noise cancellation and statistical control," *IEEE Trans. Ind. Electron.*, vol. 55, no. 12, pp. 4260–4269, Dec. 2008.
[16] J. Antoni, "Fast computation of the kurtogram for the detection of transient faults," *Mech. Syst. Signal Process.*, vol. 21, no. 1, pp. 108–124, 2007.

[17] J. Antoni and R. Randall, "Unsupervised noise cancellation for vibration signals: Part I—Evaluation of adaptive algorithms," *Mech. Syst. Signal Process.*, vol. 18, no. 1, pp. 89–101, 2004.
[18] J. Antoni and R. Randall, "Unsupervised noise cancellation for vibration signals: Part II—A novel frequency-domain algorithm," *Mech. Syst. Signal Process.*, vol. 18, no. 1, pp. 103–117, 2004.
[19] H. Ocak and K. A. Loparo, "Estimation of the running speed and bearing defect frequencies of an induction motor from vibration data," *Mech. Syst. Signal Process.*, vol. 18, no. 3, pp. 515–533, 2004.
[20] J. Wang, L. Qiao, Y. Ye, and Y. Chen, "Fractional envelope analysis for rolling element bearing weak fault feature extraction," *IEEE/CAA J. Automatica Sinica*, vol. 4, no. 2, pp. 353–360, Apr. 2017.
[21] P. Perona and J. Malik, "Scale-space and edge detection using anisotropic diffusion," *IEEE Trans. Pattern Anal.Mach. Intell.*, vol. 12, no. 7, pp. 629–639, Jul. 1990.
[22] Y. Li, Y. Ding, and T. Li, "Nonlinear diffusion filtering for peak-preserving smoothing of a spectrum signal," *Chemometrics Intell. Laboratory Syst.*, vol. 156, pp. 157–165, 2016.
[23] A. S. Raj and N. Murali, "Early classification of bearing faults using morphological operators and fuzzy inference," *IEEE Trans. Ind. Electron.*, vol. 60, no. 2, pp. 567–574, Feb. 2013.
[24] N. Nikolaou and I. Antoniadis, "Application of morphological operators as envelope extractors for impulsive-type periodic signals," *Mech. Syst. Signal Process.*, vol. 17, no. 6, pp. 1147–1162, 2003.
[25] W. Qiao and D. Lu, "A survey on wind turbine condition monitoring and fault diagnosis—Part I: Components and subsystems," *IEEE Trans. Ind. Electron.*, vol. 62, no. 10, pp. 6536–6545, Oct. 2015.
[26] G. Gerig, O. Kubler, R. Kikinis, and F. A. Jolesz, "Nonlinear anisotropic filtering of MRI data," *IEEE Trans. Med. Imag.*, vol. 11, no. 2, pp. 221–232, Jun. 1992.
[27] E. Michel-González, M. H. Cho, and S. Y. Lee, "Geometric nonlinear diffusion filter and its application to X-ray imaging," *BioMedical Eng. OnLine*, vol. 10, no. 1, Jun. 2011, Art. no. 47.
[28] Acoustics and vibration database. Accessed: Feb. 2, 2019. [Online]. Available: http://data-acoustics.com/measurements/bearing-faults/bearing-1/

Zepeng Liu (S'18) received the B.Eng. degree in electrical engineering and electronics from the University of Liverpool, Liverpool, U.K., in 2015, and the M.S. degree in power systems engineering from University College London (UCL), London, U.K., in 2016. He is currently working toward the Ph.D. degree in electrical and electronic engineering with the University of Manchester, Manchester, U.K.

His research interests include wind turbine condition monitoring and fault diagnosis, time-frequency representation, sparse representation, and data-driven analysis.

Long Zhang (M'13) received the B.Eng. and the M.Eng. degrees in electrical engineering and automation from the Harbin Institute of Technology, Harbin, China, in 2008 and 2010, respectively, and the Ph.D. degree in electronics, electrical engineering and computer science from Queen's University, Belfast, U.K., in 2013.

He was a Research Associate with the Department of Automatic Control and Systems Engineering, the University of Sheffield, Sheffield, U.K., from 2014 to 2015. He joined the Department of Electrical and Electronic Engineering, the University of Manchester, Manchester, U.K., as a Lecturer, in 2015. His research interests include machine and statistical learning, neural networks, system identification, frequency analysis, intelligent control and their applications to complex systems modeling, analysis, prediction, control, and fault diagnosis, and wind turbine condition monitoring and fault diagnosis.